REVIEW ARTICLE

Check for updates

Improving the stability of inverted perovskite solar cells towards commercialization

Bowei Li [1] & Wei Zhang [1✉]

Inverted perovskite solar cells (IPSCs) have great potential for commercialization, in terms of compatibility with flexible and multijunction solar cells. However, non-ideal stability limits their entry into the market. To shed light on the unstable origins of IPSCs, an analysis of recent research progress is needed. Here, we systematically discuss the stability of IPSCs, including each functional layer, interface and entire device, and consider environmental and operational stressors. We summarize a range of strategies for improving device stability and discuss the significance of stability test protocols. Finally, we highlight the shortcomings of current approaches for stability improvement and assessment, and provide recommendations for improving the stability of IPSCs.

Renewable energy has been increasing its share in the electricity grid due to the target of net-zero emissions, alongside the rapid growth of solar power[1]. To further reduce the levelized cost of electricity (LCOE) of solar technologies, metal halide perovskite solar cells (PSCs) are emerging candidates in next-generation photovoltaics (PVs). Of all types, inverted PSCs (IPSCs), with a positive-intrinsic-negative (p-i-n) structure, exhibit many benefits, such as diversified material choices, negligible hysteresis, and growing power conversion efficiencies (PCEs, see in Fig. 1a and Table 1)[2–6]. When incorporated into tandem cells, the inverted configuration has fewer parasitic absorption losses than the mesoporous or regular (n-i-p) counterparts[7], conferring the PCEs (Fig. 1b) of perovskite/Si (approaching 30%) and perovskite/perovskite (26.4%) surpassed the single crystal Si solar cell (26.1%) or even its theoretical maximum (29.4%)[8,9]. Thanks to the high tolerance to high-energy radiation than Si[10–12], perovskite/Cu(In, Ga)Se$_2$ (CIGS) tandem cells (with a PCE of 24.2%, higher than CIGS of 23.4%) have a promising future in space application.

In terms of mass production, the IPSCs are compatible with upscaling manufacturing that can construct the whole device by scalable solution-based processing or vapor-phase evaporation (increased PCEs and areas of minimodules are shown in Fig. 1c)[13]. Coupled with low-temperature attributes (normally below 130 °C), the IPSCs are suitable for flexible substrates and roll-to-roll processes, contributing to wearable, portable and ultra-light electronics[14,15]. In addition to these advantages, the stability of IPSCs has improved significantly in recent years, with enhanced robustness against operational stressors[16]. For example, IPSCs could maintain 96.8% of the initial PCEs after 1200 h at 65 °C[17] or have no efficiency loss after 1000 h (40 °C in a nitrogen atmosphere)[3] during the maximum power point tracking (MPPT). Under open-circuit condition (~0.76 Sun in ambient air at 85 °C), IPSCs showed a T_{95} (retained 95% of the post-burn-in efficiencies) of 1200 h[16]. More encouragingly, IPSCs have passed the industrial damp-heat test most recently[6]. Thus, a timely review focusing on the stability progress is highly necessary considering the rapid development of IPSCs.

In this Review, we aim to discuss the current challenges and future opportunities of IPSCs based on rigid substrates and hybrid three-dimensional (3D) lead perovskite, albeit the all-inorganic perovskites[18], 2D perovskites[19], and tin-based perovskites[20,21] are studied elsewhere. We first review the advance of stability research conducted on the IPSCs, starting from each

[1] Advanced Technology Institute, Department of Electrical and Electronic Engineering, University of Surrey, Guildford, Surrey GU2 7XH, UK.
✉email: wz0003@surrey.ac.uk
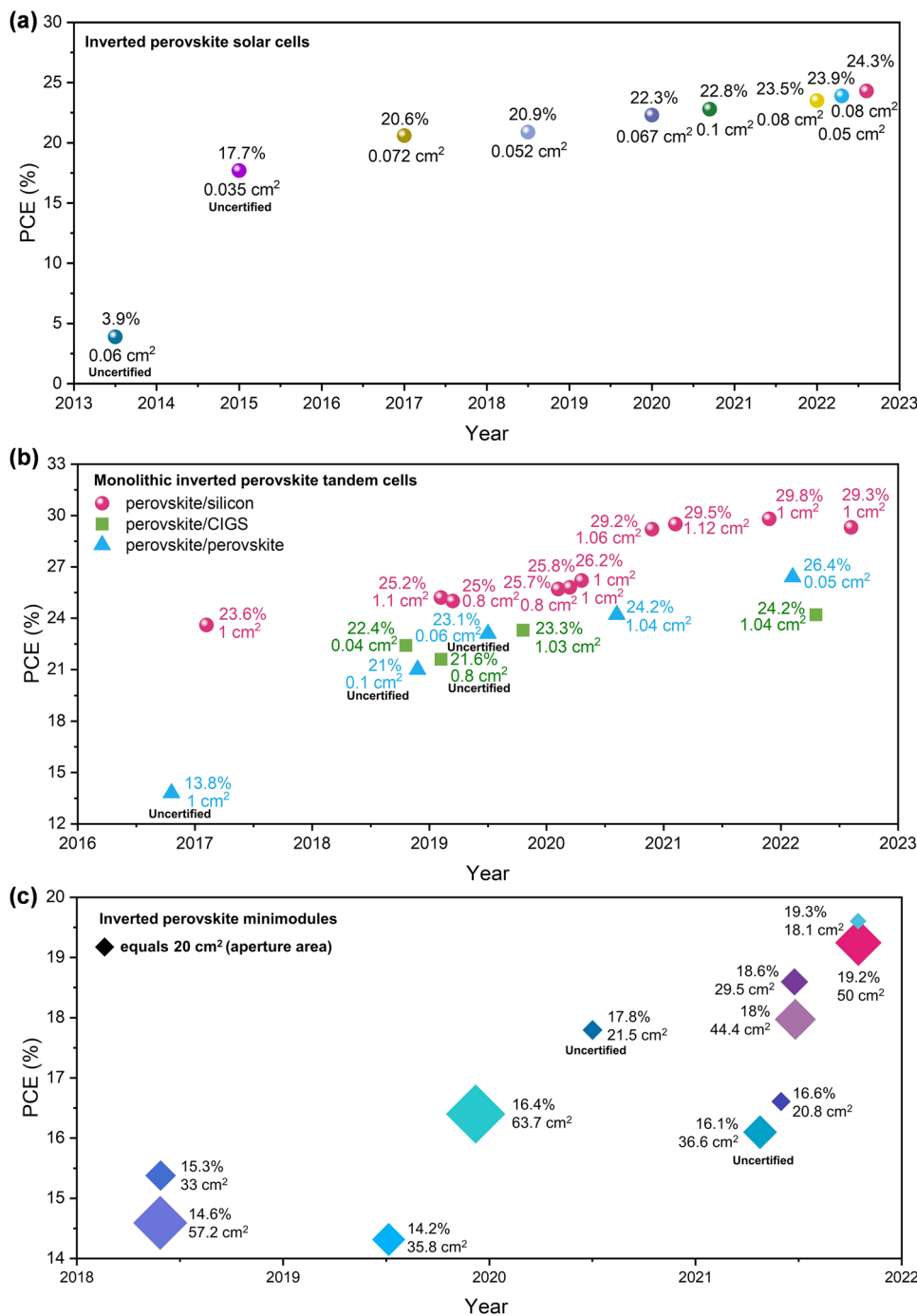
Fig. 1 The efficiency summary of IPSCs. Evolution of **a** Small-area single-junction cells. **b** Tandem cells. **c** Minimodules. Note that the inset symbol in (**c**) is proportional to the actual aperture areas (AAs). Aside from the separately labeled, the PCEs and AAs are all certified, and the details can be found in Table 1.

functional layer, such as electrodes, charge transport layers, perovskite light absorbers, and the interfaces thereof, to the entire devices under environmental or operational stressors. The following section lists a series of strategies to improve the stability of IPSCs, including small-area devices, tandem cells, and minimodules. A better understanding of these approaches would provide insights into their commercialization pathways. The next focus is on the stability assessment of IPSCs, in which the details of MPPT are compared. The final section offers our concerns about the current stability protocols and perspectives for future research and development.

Stability of each functional layer and interface

To make a good knowledge of stability in IPSCs, we would like to disassemble the device into two parts: functional layers and interfaces. As shown in Fig. 2a, a conventional IPSC is generally composed of six functional layers and five interfaces. In a typical fabrication process, a p-type hole transport layer (HTL), a perovskite light absorber, and an n-type electron transport layer (ETL) are deposited in order. Also, an additional buffer layer is required between an ETL and a metal electrode. These functional layers have diversified material choices as illustrated in Fig. 2b, most of which are coming from commercial candidates and can

Table 1 The evolution of IPSCs, consisting of small-area single-junction cells, tandem cells, and high-performance perovskite minimodules (over 14% PCEs).

Structure	AA (cm^2)	PCE (%)	Ref.
a. Single-junction cells (full cell)			
ITO/PEDOT: PSS/MAPbI$_3$/C$_{60}$/BCP/Al	0.06	3.9	[22]
FTO/PEDOT: PSS/MAPbI$_3$/C$_{60}$/BCP/Al	0.035	17.7	[23]
ITO/PTAA/FA$_{0.85}$MA$_{0.15}$Pb(I$_{0.85}$Br$_{0.15}$)$_3$/C$_{60}$/BCP/Cu	0.072*	20.6*	[24]
ITO/PTAA/(FA$_{0.95}$PbI$_{2.95}$)$_{0.85}$(MAPbBr$_3$)$_{0.15}$/PCBM/C$_{60}$/BCP/Cu	0.052*	20.9*	[2]
ITO/PTAA/Cs$_{0.05}$(FA$_{0.92}$MA$_{0.08}$)$_{0.95}$Pb(I$_{0.92}$Br$_{0.08}$)$_3$/C$_{60}$/BCP/Cu	0.067*	22.3*	[3]
ITO/PTAA/Cs$_{0.05}$(FA$_{0.95}$MA$_{0.05}$)$_{0.95}$Pb(I$_{0.95}$Br$_{0.05}$)$_3$/C$_{60}$/BCP/Ag	0.1*	22.8*	[4]
ITO/PTAA/MA$_{0.6}$FA$_{0.4}$PbI$_3$/C$_{60}$/BCP/Ag	0.07	23.8	[25]
ITO/P3CT-N/(FAPbI$_3$)$_{0.95}$(MAPbBr$_3$)$_{0.05}$/PCBM/C$_{60}$/TPBi/Cu	0.08*	23.5*	[5]
ITO/2PACz/MA$_x$FA$_{1-x}$PbI$_3$/C$_{60}$/BCP/Ag	0.07	24.3	[6]
ITO/NiO$_x$/Cs$_{0.05}$FA$_{0.85}$MA$_{0.1}$PbI$_3$/C$_{60}$/BCP/Ag	0.05*	23.9*	[26]
ITO/PTAA/Cs$_{0.05}$(FA$_{0.98}$MA$_{0.02}$)$_{0.95}$Pb(I$_{0.95}$Br$_{0.02}$)$_3$/C$_{60}$/BCP/Ag	0.08*	24.3*	[27]
b. Monolithic tandem cells			
Perovskite/Si (top cell)			
ITO/NiO$_x$/Cs$_{0.2}$FA$_{0.8}$PbI$_{2.84}$Br$_{0.16}$/LiF/PCBM/SnO$_2$/ZTO/ITO/LiF/Ag	1*	23.6*	[7]
ITO/poly-TPD/NPD/Cs$_{0.05}$(FA$_{0.83}$MA$_{0.17}$)$_{0.95}$Pb (I$_{0.82}$Br$_{0.18}$)$_3$/PCBM/BCP/Ag	1.1*	25.2*	[28]
ITO/PTAA/MA$_x$FA$_{1-x}$PbI$_{1-x}$Br$_x$/C$_{60}$/SnO$_2$/IZO/LiF/Ag	0.8*	25*	[29]
ITO/NiO$_x$/Cs$_{0.05}$MA$_{0.15}$FA$_{0.8}$PbI$_{2.25}$Br$_{0.75}$/C$_{60}$/SnO$_x$/IZO/MgF$_2$/Ag	0.8*	25.7*	[30]
ITO/NiO$_x$/poly-TPD/PFN-Br/(Cs$_{0.22}$FA$_{0.78}$Pb(I$_{0.85}$Br$_{0.15}$)$_3$)$_{0.97}$(MAPbCl$_3$)$_{0.03}$/LiF/C$_{60}$/SnO$_2$/ZTO/ITO/Ag/PDMS	1*	25.8*	[31]
ITO/PTAA/FA$_{0.65}$MA$_{0.20}$Cs$_{0.15}$Pb(I$_{0.8}$Br$_{0.2}$)$_3$/C$_{60}$/PEIE/ITO/Ag	1*	26.2*	[32]
ITO/Me-4PACz/MA$_x$FA$_{1-x}$PbI$_{1-x}$Br$_x$/LiF/C$_{60}$/SnO$_2$/IZO/LiF/Ag	1.06*	29.2*	[9]
/	1.12*	29.5*	[33]
/	1*	29.8*	[34]
ITO/2PACz/Cs$_{0.05}$FA$_{0.8}$MA$_{0.15}$Pb(I$_{0.755}$Br$_{0.255}$)$_3$/MgF$_x$/C$_{60}$/SnO$_2$/IZO/Ag	1*	29.3*	[35]
Perovskite/CIGS (top cell)			
ITO/PTAA/Cs$_{0.09}$FA$_{0.77}$MA$_{0.14}$Pb(I$_{0.86}$Br$_{0.14}$)$_3$/PCBM/ZnO/ITO/MgF$_2$	0.04*	22.4*	[36]
ITO/NiO$_x$/PTAA/Cs$_{0.05}$(MA$_{0.17}$FA$_{0.83}$)$_{0.95}$Pb(I$_{0.83}$Br$_{0.17}$)$_3$/C$_{60}$/SnO$_2$/IZO/Ag/LiF	0.8	21.6	[37]
AZO/MeO-2PACz/Cs$_{0.05}$(MA$_{0.17}$FA$_{0.83}$)$_{0.95}$Pb(I$_{0.83}$Br$_{0.17}$)$_3$/C$_{60}$/SnO$_2$/IZO/LiF/Ag	1.03*	23.3*	[38]
AZO/Me-4PACz/Cs$_{0.05}$(MA$_{0.23}$FA$_{0.77}$)$_{0.95}$Pb(I$_{0.77}$Br$_{0.23}$)$_3$/LiF/C$_{60}$/SnO$_2$/IZO/LiF/Ag	1.04*	24.2*	[39]
Perovskite/perovskite (full cell)			
ITO/NiO$_x$/FA$_{0.83}$Cs$_{0.17}$Pb(I$_{0.5}$Br$_{0.5}$)$_3$/PCBM/SnO$_2$/ZTO/ITO/PEDOT:PSS/FA$_{0.75}$Cs$_{0.25}$Pb$_{0.5}$Sn$_{0.5}$I$_3$/C$_{60}$/BCP/Ag	1	13.8	[40]
ITO/PTAA/FA$_{0.8}$Cs$_{0.2}$Pb(I$_{0.7}$Br$_{0.3}$)$_3$/C$_{60}$/BCP/Ag/MoO$_x$/ITO/PEDOT: PSS/(FASnI$_3$)$_{0.6}$(MAPbI$_3$)$_{0.4}$/C$_{60}$/BCP/Ag	0.1	20.6	[41]
ITO/NiO$_x$/poly-TPD/PFN-Br/FA$_{0.6}$Cs$_{0.3}$DMA$_{0.1}$PbI$_{2.4}$Br$_{0.6}$/LiF/C$_{60}$/PEIE/AZO/IZO/PEDOT:PSS/FA$_{0.75}$Cs$_{0.25}$Sn$_{0.5}$Pb$_{0.5}$I$_3$/C$_{60}$/BCP/Au	0.06	23.1	[42]
ITO/NiO$_x$/VNPB/FA$_{0.8}$Cs$_{0.2}$Pb(I$_{0.6}$Br$_{0.4}$)$_3$/C$_{60}$/SnO$_2$/Au/PEDOT:PSS/FA$_{0.7}$Cs$_{0.3}$Sn$_{0.5}$Pb$_{0.5}$I$_3$/C$_{60}$/SnO$_2$/Cu	1.04*	24.2*	[43]
ITO/NiO$_x$/VNPB/FA$_{0.8}$Cs$_{0.2}$Pb(I$_{0.62}$Br$_{0.38}$)$_3$/C$_{60}$/SnO$_2$/Au/PEDOT:PSS/FA$_{0.7}$Cs$_{0.3}$Sn$_{0.5}$Pb$_{0.5}$I$_3$/C$_{60}$/SnO$_2$/Cu	0.05*	26.4*	[44]
c. Minimodules (full cell)			
ITO/PTAA/MAPbI$_3$(blade coating)/C$_{60}$/BCP/Cu	33*	15.3*	[45]
	57.2*	14.6*	
FTO/NiO$_x$/MAPbI$_3$(slot-die coating)/G-PCBM/BCP/Ag	35.8*	14.2*	[46]
ITO/PTAA/MAPbI$_3$(blade coating)/C$_{60}$/BCP/Cu	63.7*	16.4*	[47]
ITO/PTAA/MAPbI$_3$(blade coating)/C$_{60}$/BCP/Cu	21.5	17.8	[48]
TO/P3HT-COOH/MAPbI$_3$(spin coating and dipping)/C$_{60}$/BCP/Au	36.6	16.1	[49]
FTO/NiMgLiO/FA$_{0.83}$Cs$_{0.17}$PbI$_{2.83}$Br$_{0.17}$(slot-die coating)/C$_{60}$/BCP/Bi/Ag	20.8*	16.6*	[13]
ITO/PTAA/FA$_{0.92}$Cs$_{0.08}$PbI$_3$(blade coating)/C$_{60}$/BCP/Cu	29.5*	18.6*	[50]
	44.4*	18*	
ITO/PTAA/MA$_{0.6}$FA$_{0.4}$PbI$_3$(blade coating)/C$_{60}$/BCP/Cu	18.1*	19.2*	[25]
	50*	19.3*	

Note that the table includes the device structures, aperture areas (AA), champion PCEs and references (Ref.). The asterisk indicates the certified values.

be prepared by solution processing with low temperatures. In addition to intrinsic properties (physical, chemical, or structural issues), the stability of functional layers and interfaces can be also evaluated by the performance stability of the fabricated devices. For entire devices, there are many factors, also called stressors, influencing the device lifetime as summarized in Fig. 2c. Based on these multiple stressors, the material stability of each functional layer and the operational stability of IPSC devices will be emphasized in the following discussion.

Electrode layer. The electrodes (the bottom and top) are typically made of transparent conductive oxide (TCO) and metal contact,

respectively. The bottom TCO not only supports the thin-film deposition but also acts as the anode in IPSCs. For TCO electrodes, indium tin oxide (ITO) and fluorine-doped tin oxide (FTO) coated glass are the two main types of rigid substrates. Unlike FTO with higher resistance of temperature, the ITO is more frequently used in IPSCs due to the better transmittance at a given conductivity[51] and low-temperature requirement for solution-processed HTLs. Although the ITO is relatively stable (lower thermal expansion coefficients[52]) compared to other functional layers, there is still potential to improve the device stability by modifying the ITO. Our recent work discloses that replacing ITO with single-walled carbon nanotubes (SWCNTs) can further improve the environmental and mechanical stability
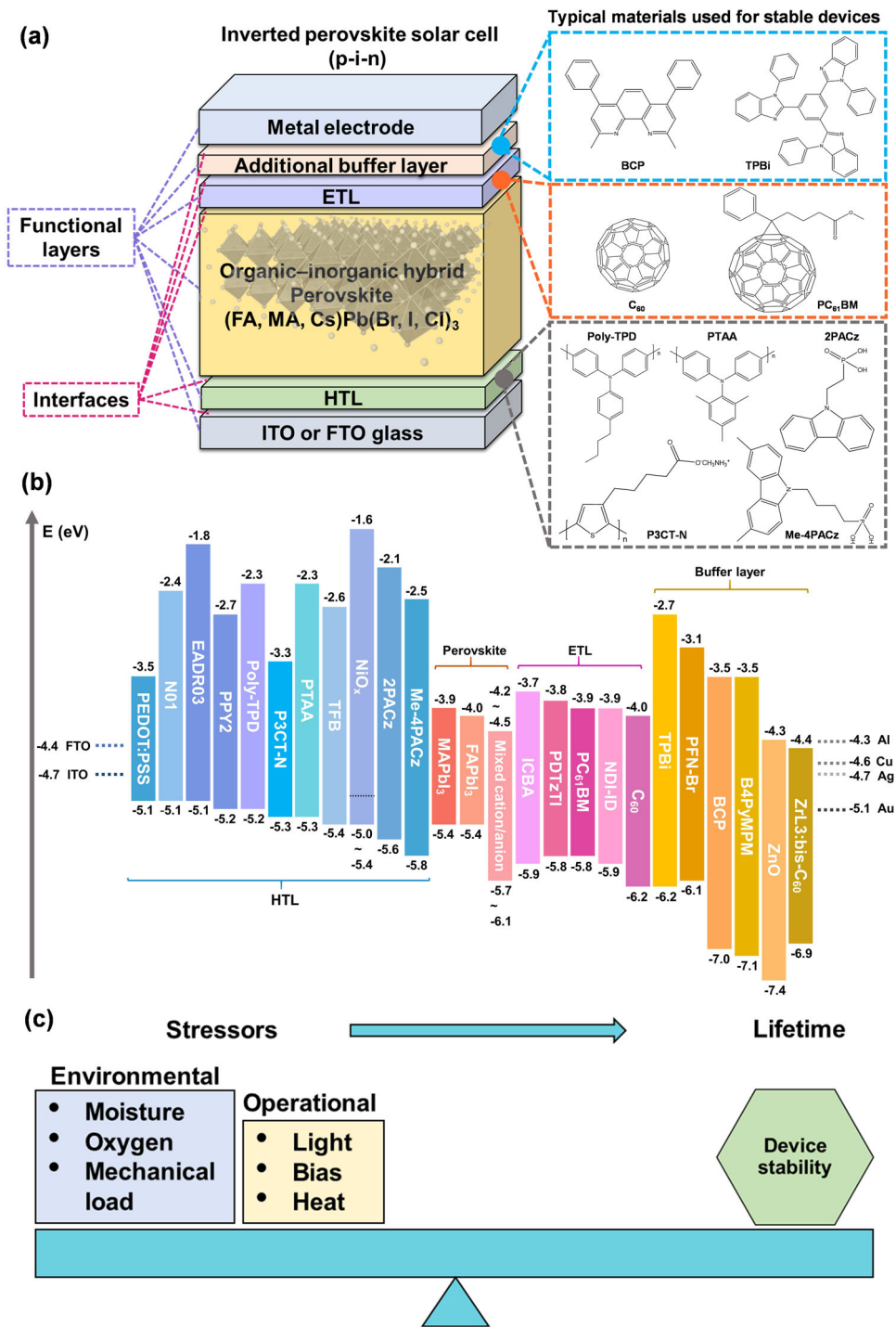
Fig. 2 Overview of IPSCs. a Schematic configuration and corresponding materials for functional layers. Note that HTL denotes the hole transport layer. ETL denotes the electron transport layer. ITO denotes indium tin oxide and FTO denotes fluorine-doped tin oxide. The IPSCs based on the exhibited materials showed both high efficiency and long stability. **b** Energy level diagram of functional layers in high-performance IPSCs. **c** The stressors affecting the device lifetime, including environmental and operational stressors.

of the fabricated devices[53]. The top electrode (cathode) is normally evaporated by metals, such as Ag, Cu, Au, Al[54–56]. These materials are widely used thanks to their good electric conductivity whilst chemical-stability issues are also encountered. Al is less stable than other candidates in the air according to the reactivity order. Ag and Au could go through the charge transport layer to form "metal halide" with the perovskites because of the ion-diffusion process[57,58]. Cu can be oxidized by moisture and oxygen and the products of $Cu(OH)_2$ or CuO_x would also react

with the perovskite[56]. Based on the performance data, Au-based IPSC devices show excellent operational stability under 85 °C[16,59], but the high cost will inhibit its wide application. From an economic perspective, Cu is a favorable candidate for large-area perovskite devices (see in Table 1). Moreover, non-metal materials (like carbon[60], ITO[58], Al-doped zinc oxide (AZO)[61], and indium zinc oxide (IZO)[3]), are useful for thermal stability although the devices would sacrifice efficiency due to the increased series resistance. Besides, these transparent electrodes

are essential in the fabrication of perovskite tandem cells while the complex processing may inhibit their application in large modules.

Hole transport layer (HTL). Although HTL-free structure has been reported[62], the HTL is indispensable for highly stable IPSCs[16,25]. The most famous hole transport material, 2,2′,7,7′-Tetrakis[N,N-di(4-methoxyphenyl)amino]-9,9′-spirobifluorene (spiro-OMeTAD), cannot be applied in IPSCs because of its solubility in perovskite solvents[63]. Nevertheless, there are many other candidates, which are divided into inorganic and organic categories. For inorganic HTLs, nickel oxide (NiO_x) achieved a higher device efficiency than other materials[26]. However, in terms of the chemical property, the NiO_x is a photo-catalyst and prone to be Ni_2O_3[64], indicating less stability under light and oxygen[65]. Also, the NiO_x device showed inferior stability induced by electrical bias[66] or thermal heating (85 °C testing in nitrogen)[16]. This might be ascribed to the high defects concentration of NiO_x that the $Ni^{\geq 3+}$ would interact with the perovskite, leading to severe interfacial recombination[67,68]. Therefore, the organic HTLs are essential to be introduced, yielding the champion efficiency of 24.3% (certified) in the IPSCs[27]. Poly (3,4-ethylene dioxythiophene):poly(styrenesulfonate) (PEDOT: PSS) is the first HTL used in IPSCs[22] but its acidic and hygroscopic properties deteriorate the device durability[69]. Thus, more organic polymers were studied, such as poly[N,N′-bis(4-butylphenyl)-N,N′-bis(phenyl) benzidine] (poly-TPD)[70], poly(bis(4-phenyl)(2,4,6-trimethylphenyl)amine) (PTAA)[63], and poly[3-(4-methylamine carboxylbutyl) thiophene] (P3CT-N)[5], all of which showed excellent device efficiencies and performance stability in lab-scale devices or minimodules. In recent years, self-assembled organic materials have emerged increasingly, like [2-(9H-carbazol-9-yl)ethyl] phosphonic acid (2PACz)[38], poly[3-(6-carboxyhexyl)thiophene-2,5-diyl] (P3HT-COOH)[71], 4′-(3,6-bis(2,4-dimethoxyphenyl)-9H-carbazol-9-yl)-[1,1′-biphenyl]-4-carboxylic acid (EADR04)[72], and [4-(3,6-dimethyl-9H-carbazol-9-yl)butyl]phosphonic acid (Me-4PACz)[9], with excellent performance stability in single junction[6] and tandem cells[9,35].

Perovskite light absorber. The hybrid three-dimensional (3D) lead perovskite with a formula of $APbX_3$ (A denotes organic or inorganic cations and X denotes halide anions) is still the mainstream in IPSCs. To fabricate perovskite thin films, various deposition methods have been created while solution processing is still one of the best choices for future commercialization. Aside from processing in extremely low-humidity and oxygen conditions (like in a glove box, dry box, or vacuum chamber), the growth of perovskite thin film can be conducted in ambient conditions with controlled humidity. The most recent study displayed a certified PCE of 23.5% based on the annealing process in the air (relative humidity, RH: 30–40%)[5]. However, perovskite stability is still the key issue since the as-crystallized perovskite will decompose in the presence of water and oxygen[73]. Also, due to the ionic and polycrystalline nature, the perovskite film inevitably contains numerous defects that further accelerate the aging process. For example, halide vacancies could trap oxygen to form superoxide radicals under illumination[74], which is detrimental to the perovskite film.

Electron transport layer (ETL) and buffer layer. The fullerene ETLs are predominant for high-performance devices, mainly consisting of C_{60} and [6,6]-phenyl-C_{61}-butyric acid methyl ester ($PC_{61}BM$, abbreviated as PCBM in the following section). Thanks to the Lewis-acid property, these two fullerene materials can passivate electron-rich defects in perovskite[75]. With complementary passivation, double-fullerene layers (PCBM and C_{60}) were frequently adopted to suppress traps[76], retarding the intrusion of water and oxygen to some extent. The recent IPSCs based on mere PCBM or C_{60} ETL also showed excellent operational stability[6,16]. This may be due to the 'scavenging effect' of PCBM[77]. On top of ETL, introducing a buffer layer can reduce the interfacial barrier at ETL/electrode[78]. Bathocuproin (BCP) is the most common use in IPSCs, yielding the highest PCE[25] and longest operational stability[16,79]. The BCP deposition is compatible with the solution or evaporation techniques. However, thermal evaporation could cause crystalization, so the solution-processed BCP devices showed better thermal stability[50]. Furthermore, BCP can be replaced by other candidates to improve device durability, such as metal acetylacetonates[80], metal-organic frameworks[81], atomic-layer-deposition (ALD) SnO_2[3], Zn-doped SnO_2 (ZTO)[31], and organometallic complexes[82].

Interfaces. Interfaces have multifunction in IPSCs, involving energy-level alignment, charge dynamics (extraction, transfer, and recombination), defect passivation, and ion migration[83]. Thus, the imperfect contacts will induce interfacial losses and impair the device performance. From bottom to top, the first interface is located between TCO and HTL. The HTLs have a tight adhesion and low thickness (normally less than 10 nm for polymer and 1–3 nm for monolayer small molecules)[2,38], leading to challenges to study TCO/HTL interface. Also, the buffer layer (also with a thin thickness of several nanometers)[3] can be regarded as an interlayer between ETL and electrode so the interfaces between ETL/buffer layer and buffer layer/metal, are less studied. Overall, most studies focus on the adjacent interfaces of perovskite (HTL/perovskite and perovskite/ETL), because these two interfaces are prone to have high trap densities in comparison with high-quality perovskite films[84,85]. The buried interface between HTL and perovskite was found to cause most deep traps due to the sub-microscale imperfections or inhomogeneities[85,86]. Through lift-off or peel-off strategies, clear voids are observed at this interface[25]. These voids will be enlarged after several-hour light soaking, leading to device aging. In comparison with HTL/perovskite interface, the perovskite/ETL interface has severe non-radiative recombination when using fullerene ETLs[87]. In addition, the ion diffusion from perovskite to metal electrode (bilateral process) is the other factor affecting the device stability.

Strategies for improving the stability of IPSCs

To improve the stability of IPSCs, many strategies have been investigated, such as materials engineering of charge transport layers (CTLs) or electrodes, compositional engineering of perovskites, and interface engineering of whole devices. In this section, we will discuss these approaches in more detail. The above layer-by-layer discussion indicates that the intrinsic stability of IPSCs is closely related to each functional layer, in particular for the CTLs. For bottom HTLs, organic materials are more beneficial for stability based on the present device performances[5,6,16]. This could be attributed to their unique properties. Specifically, the cross-linking process of polymer HTLs enhances the resistance of solvent, moisture, and mechanical stress[88]. The self-assemble process between small organic molecules and TCO increases the cohesion and adhesion toughness (low fracture energy, G_c, $J\,m^{-2}$)[72,89]. Thus, both polymer and small organic-molecule HTLs show excellent operational stability[5,6,16]. For top ETLs, modified C_{60} and PCBM enabled the devices to improve moisture stability. For example, the cross-linkable silane with C_{60} (C_{60}-SAM)[90] or PCBM-derived electrolyte (PCBB-3N-3I)[91] enhances the water resilience but it still needs to combine with
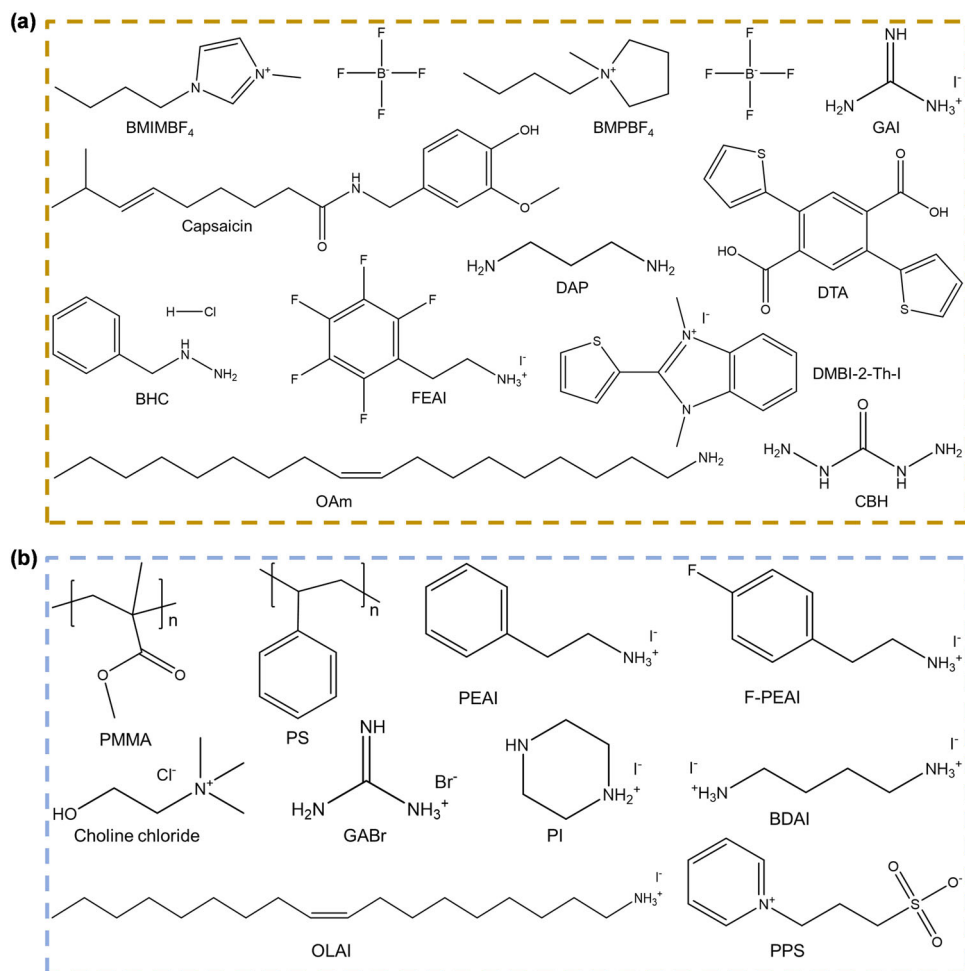
Fig. 3 Typical organic structures for stable IPSCs. a Chemicals added in perovskite. **b** Chemicals applied at interfaces between the perovskite and charge transport layers. Note that the chemicals of the top row (PMMA, PS, PEAI, F-PEAI) in (**b**) can be applied in different interfaces, such as the HTL/perovskite and perovskite/ETL.

the pure C_{60} or PCBM in the fabrication of devices. For pure ETLs, non-fullerene substitutes were found to improve thermal stability. Small rylene diimide molecules, like N,N'-Bis(1-indanyl) naphthalene-1,4,5,8-tetracarboxylic diimide (NDI-ID)[92], and N-type conjugated polymer, like poly(2,2'-bithiazolothienyl-4,4',10,10'-tetracarboxydiimide) (PDTzTI)[93], achieved PCEs over 20% with better thermal stability than PCBM based devices. Hence, the material design of ETLs is the breakthrough for device stability although the C_{60} and PCBM are irreplaceable for the state-of-the-art high-performance IPSCs.

In addition to CTLs, the perovskite light absorber is still the key component. Finding means to increase the intrinsic stability of perovskite bulk film will prolong the device lifetime. Compositional engineering (tunning $APbX_3$ or introducing additives) is a straightforward method, in which the A sites can affect the perovskite stability. Formamidinium (FA, $CH_3(NH_2)_2^+$) or cesium (Cs^+) is known to be more thermal stable than methylammonium (MA, $CH_3NH_3^+$). The mixed A-site perovskites, such as MAFA, CsFA, CsMAFA, could further increase the phase, photo, moisture, and thermal stability compared to the pure FA perovskite[94]. Therefore, the multi-cation compositions constitute perovskite light absorbers in most stable IPSCs[2,3,6,16]. Moreover, non-stoichiometric perovskite precursors also showed advantages. Apart from excess PbI_2 (0.5–1 mol%[2]), recent studies found that adding AX in perovskite precursor can suppress redox reactions between the perovskite and NiO_x[68] and enhance the

photostability of $FA_xCs_{1-x}PbI_3$ perovskite film[50]. To further improve the operational stability, a series of ligands and additives were introduced in perovskite precursors, such as alkylamine[3] and ionic liquid salts (Fig. 3a)[16,59]. According to the device data, the ligands design would be a useful aspect to enhance the perovskite stability.

The optimized interfaces could further delay the device degradation and extend the operational lifetime. Thanks to facile processing, interface engineering is widely adopted in IPSCs. As summarized in Table 2, numerous passivation agents (modulators or passivators, also seen in Fig. 3b) were introduced in the fabricated devices, such as post-treatments that resided on the perovskite surface. In addition to physical methods (microwave annealing[95] and mechanically peeling off[96]), introducing hydrophobic insulating polymer (electron can transport from perovskite to ETL through tunneling effect) could significantly increase water or moisture resistance[97]. Also, the reacted capping layer (sulfidation[5] or oxidation[17] with excess lead source) can improve the operational stability since it significantly inhibited ion migration or diffusion under illumination. Even for the encapsulated devices, this ion-diffusion process is inevitable and thus many barrier layers were introduced between the buffer layer and metal electrode, such as Cr/Cr_2O_3[57,59], bismuth (Bi)[98], benzotriazole (BTA)[99]. Moreover, a recent study found that two-dimensional (2D) perovskite layers (Ruddlesden-Popper phase, post-treated by oleylammonium iodide) can prolong the

Table 2 The summary of instability origins and corresponding strategies to improve the stability of IPSCs (based on rigid substrates).

Instability origins	Strategies
Small-area cells or minimodules (single junction)	
TCO and metal electrode	• Replace ITO substrate with single-walled carbon nanotubes (SWCNTs)[53]. • Use electrode mixture, like Cu-Ag bilayers[101]. • Introduce barrier layers: such as **Cr/Cr$_2$O$_3$**[57,59], Bi[98], benzotriazole (BTA)[99]. • Use non-metal materials: carbon[60], **inidium zinc oxide (IZO)**[3], **ITO**[58], Al-doped zinc oxide (AZO)[61]. • Use parallel interconnection to avoid second scribing (P2) contacts with the perovskite[13]. • Introduce low-dimensional diffusion barriers to prevent vertical and lateral diffusion of iodide ions[46].
Buffer layer	• Use new layers: such as **ALD-SnO$_2$**[3], Zn-doped SnO$_2$ (ZTO)[31], metal acetylacetonates[80], metal-organic frameworks[81], and organometallic complexes[82]. • Adapt **solution processing** to avoid the crystallization of BCP in thermal evaporation[50].
Electron transport layer (ETL)	• Use **double-fullerene layers** (PCBM and C$_{60}$)[76]. • Replace fullerene ETL with small molecules, like *N,N′*-Bis(1-indanyl)naphthalene-1,4,5,8-tetraca-rboxylic diimide (NDI-ID)[92]. • Replace fullerene ETL with polymer, like poly(2,2′-bithiazolothienyl-4,4′,10,10′-tetracarb-oxydiimide) (PDTzTI)[93].
Perovskite layer	• Add ionic liquid salts in perovskite precursor, e.g., **1-butyl-3-methylimidazolium tetrafluoroborate (BMIMBF$_4$)**[59], 1-butyl-1-methylpiperidinium tetrafluoroborate (BMPBF$_4$)[16]. • Convert the surfaces to water-insoluble lead (II) oxysalt[17] and sulfidation[5], or moisture-resistance 2D perovskite[6]. • Introduce additives to reduce the defects and improve film quality: guanidinium iodide (GAI)[102], capsaicin[103], heavy water or deuterium oxide (D$_2$O)[104], star-shaped polymer[105], oleylamine (OAm)[3], 1,3-diamino-propane (DAP)[106], 2,5-di(thiophen-2-yl)terephthalic acid (DTA)[107], 1,3-dimethyl-2-thiophen-2-yl)-2,3-dihydro-1*H*-benzo[d]imida-zole (DMBI-2-Th) and its iodine ionized molecule DMBI-2-Th-I[108], 2-(2,3,4,5,6-pentafluorophenyl)ethylammonium iodide (FEAI)[109]. • Add benzylhydrazine hydrochloride (BHC) in perovskite to reduce the oxidization of iodide ions[110]. • Add excessive FAI and CsI in FA$_x$Cs$_{1-x}$PbI$_3$ perovskite to improve film photostability[50]. • Partially replace DMSO with carbohydrazide (CBH) to remove voids[25]. • Physical treatments: microwave annealing process[95], mechanically peel off by adhesive tapes[96].
Hole transport layer (HTL)	• Use polymer hole transport layer, such as as **poly[*N,N′*-bis(4-butylphenyl)-*N,N′*-bis(phen-yl)benzidine] (poly-TPD)**[70], **poly(bis(4-phenyl)(2,4,6-trimethylphenyl)amine) (PT-AA)**[63], **poly[3-(4-methylamine carbo-xylbutyl) thiophene] (P3CT-N)**[5], poly[(9,9-dioctyl-fluorenyl-2,7-diyl)-co-(4,4′-(N-(4-sec-butylphenyl) diphenylamine)] (TFB)[111], pyridine-based polymer (PPY2)[112], donor-π-linker-donor (D-π-D) molecule (N01)[113]. • Use self-assembled monolayer, such as **[2-(9H-carbazol-9-yl)ethyl]phosphonic acid (2PACz)**[38], 4′-(3,6-bis(2,4-dimethoxyphenyl)-9H-carbazol-9-yl)-[1,1′-biphenyl]-4-carboxylic acid (EADR04)[72], COOH-functionalized P3HT (P3HT-COOH)[71]. • Spin coat Mg-organic (MgO(R)), like Mg(AcO)$_2$•4H$_2$O on NiO$_x$ to remove dark hysteresis[66]. • Add excess A-site in perovskite precursor or ionic liquid into NiO$_x$[114] to suppress redox reactions between the perovskite and NiO$_x$[68]. • Add dimethylammonium iodide (DMAI) in perovskite precursor to reduce lattice disorder and defects at the perovskite/NiO$_x$ interface[67].
Interface	For top interface (perovskite/ETL): • C$_{60}$ derivative (e.g., PCBB-3N-I[91]). • **Zwitterion**[24] (e.g., L-α-phosphatidyl-choline, choline chloride). • Organic halide salts (e.g., **phenylethylammonium iodide (PEAI)**, **guanidinium bromide (GABr)**[2], piperazinium iodide (PI)[4], 4-fluoro-phenylethylammonium iodide (F-PEAI)[115], oleylammonium iodide (OLAI)[6]. • Conjugated small molecule and polyelectrolytes (e.g., Y6[116], poly[(9,9-bis(3′-((N,N-dimethyl)-N-ethylammonium)-propyl)-2,7-fluorene)-alt-2,7-(9,9-di-octylfluorene)]diiodide (PFN-I)[84]). • Insulating polymer[97] (e.g., **polystyrene (PS)**, Teflon, poly(vinylidene fluoride-trifluoroethylene) (PVDF-TrFE), **poly(methyl methacrylate) (PMMA)**). • Hydrophobic layer (e.g., Trichloro(3,3,3-trifluoropropyl)silane[97], cross-linkable silane with C$_{60}$ (C$_{60}$-SAM)[90]). For bottom interface (HTL/perovskite): 1,4-butanediammonium iodide (BDAI)[117], 3-(1-pyridinio)-1-propanesulfonate (PPS)[118], WS$_2$[119].
Tandem cells	
Perovskite layer	• Introduce pulsed-chemical vapor deposition (CVD) processed SnO$_2$/ZTO window layer to suppress perovskite degradation under thermal and damp-heat test[7]. Photoinduced phase segregation of wide-bandgap perovskite: • Use thiol self-limiting passivation (SLP) treatment (1-butanethiol on the surface)[30]. • Add more Cl in perovskite to form triple-halide alloys[31]. • Add a mixture of thiocyanate (SCN) in perovskite[32]. • Add CsBr/FABr in perovskite precursor (six precursors showed better photostability than four precursors at the same composition ratios)[43]. • Use fast hole extraction of [4-(3,6-dimethyl-9H-carbazol-9-yl)butyl]phosphonic acid (Me-4PACz) as the hole transport layer[9].

The highlighted chemicals or methods (bold font) in the strategies have a wider report or adoption in the IPSC community.

performance stability[6]. Although 2D perovskite has low charge-carrier mobility and short diffusion length[100], the hydrophobic large cations could enable the 2D perovskite as the moisture or oxygen barrier. Also, the 2D perovskite can passivate surface defects and block ion migration, contributing to one of the best efficiencies (24.3%) and passing the standard industrial damp-heat test[6]. However, the 2D perovskite is highly dependent on the fabrication method since the oleylamine added in the perovskite precursor did not show any 2D component[3]. Hence, the detailed formation process of 2D perovskite merits further investigation.

To enhance device stability, a large number of engineering methods have been developed in the IPSCs. However, more attention should be paid to utilizing these approaches. Some interfacial layers are useful for device efficiency but detrimental to operational stability (like LiF[9]). This indicates that the passivation materials may have the opposite impact on efficiency and stability. Introducing an interlayer or agent may cause new interfaces to form inside the devices and thus increase uncertainties with the time elapsed. Long-term illumination or other stressors could induce a new reaction between the passivation agents and perovskite or CTLs. Therefore, we should be cautious of material selections in the preparation of IPSCs and be more patient in verifying the operational stability even if an obvious increase in the initial PCE.

Many of these stability approaches, albeit impressive and useful, are based on lab-scale devices and normally require precise control in the preparation process (e.g., the 2D capping layer). Besides, it is questionable whether these methods can be scaled up in the fabrication of large-area modules. Additional factors of a specific upscaling deposition method will bring new challenges to use these stability approaches. For inverted minimodules, the stability is also affected by the entire design, like the laser scribing (P1-P2-P3) interconnection[13]. Thus, a standard geometry is helpful for all researchers, rather than only defining the geometrical fill factor (GFF) for different patterns. Aside from the aforementioned functional layers, an anti-reflection coating (such as magnesium fluoride layer (MgF_2)[46] and polydimethylsiloxane (PDMS)[25]) was additionally introduced in recent high-performance cells or minimodules to increase the PCE (due to the relatively lower current density (J_{SC}) than that of the meso-porous and regular devices). However, the stability of these anti-reflective layers is yet to be investigated in IPSCs. Being exposed to the incident light directly, the anti-reflective layer requires more evidence to confirm its survival with long-term stressors.

Stability assessment of the entire device

Standardized testing protocols are prerequisites for commercialization. The stability assessments of IPSCs can learn from two mature standards: The International Summit on Stability of Organic Solar Cells (ISOS) and the International Electrotechnical Commission (IEC). The former provides various stability measurements for lab-scale devices and the latter (like IEC 61215:2016) is an industrial qualification. The IPSCs can refer to ISOS procedures, which judge the device stability at various levels, ranging from dark storage to operational stability[120]. To reflect real-world lifetime, operational stability is encouraged to be reported[121]. Of all types, maximum power point tracking (MPPT) is a typical measurement, which can simulate the operational performance by considering electrical bias, heat (self-heating effect under light source), and illumination simultaneously[120,122]. To perform the practical measurements, the detailed aging conditions need to be noted, involving the light source, bias, UV filter, temperature, atmosphere, encapsulation, device structure, initial PCE, and operational time. After years of endeavor, the

operational stability of the IPSCs has improved significantly (Table 3). The MPPT results, as shown in Fig. 4a–c, indicate that the small-area single-junction device displays only 2% drops after 1500 h. The perovskite/Si tandem cell shows a PCE of around 28% after 300 h. The minimodule still maintained 85% of initial PCE after 1000 h. In addition to ISOS procedures, a suite of IEC 61215:2016 standards is complementary for device stability even though it looks stringent for the present IPSCs. Encouragingly, the encapsulated IPSCs have passed the damp-heat test (85 °C/ 85%RH)[6], which inspires us to spend more effort on stability study and eventually push the IPSCs into the PV market.

For stability assessments, the current protocols are not sufficient under certain conditions, such as under ultraviolet (UV) light and high-level radiation exposure. According to the IEC 61215 requirement, the minimum standard for UV illumination is 15 kW h m^{-2} (irradiation from 280 to 400 nm)[123]. However, the UV-light stability of IPSCs is seldom reported. For most MPPT measurements, the illumination source normally used LEDs or a cut-off filter (at 350[72] or 420[3] nm). These lead to scarce knowledge of device stability under UV light. Thus, it is essential to investigate the UV-light stability in IPSCs since it can help to de-couple degradation mechanisms. In addition to the UV-irradiation, a high-radiation environment induced by high-charge and high-energy particles also need to be considered. The research found that NiO_x is a problematic layer in perovskite/ CIGS tandem cells under high-proton irradiation (68 MeV)[124]. However, such acute exposures cannot reflect the real conditions in the space station, Moon, Mars or even beyond, so a standard assessment for radiation degradation should be added in IPSCs. Aside from the UV or high-radiation stressor affecting the device intrinsic stability, external stability, such as encapsulation processing, also needs to be considered. Most encapsulations have so far used the methods directly from the previous PV experience, but the PSC degradation can be induced by these methods, like the electrical feedthrough (oxygen and water can diffuse) or the encapsulant itself (which may react with perovskite)[125]. The efficient encapsulations for IPSCs with long-term robustness are urgently needed. To commercialize IPSCs, real-world operation or field tests are indispensable and the IPSCs have shown promising durability. For example, the IPSC devices (initial PCEs are over 23%) show an obvious recovery after pausing 12 h in the 500 h MPPT (ISOS-L-3)[26]. Also, IPSC minimodules show superior tolerance to the shading effect (no permanent damage to the whole module when performing over 50 cycles of shading/de-shading for subcells)[47]. These characteristics indicate the excellent performance stability of IPSCs in real-world conditions.

Outlook

With the rapidly advancing device efficiency, the IPSC community faces an urgency for an in-depth understanding of the degradation mechanism. Only by resolving stability issues properly, the IPSCs would participate in the global PV market. To further develop the IPSCs toward commercialization, there are some suggestions are listed as follows.

a. We encourage researchers to report the intrinsic stability of IPSCs (unencapsulated in the air with monitored temperature and humidity, or unencapsulated in inert conditions) when performing long-term operational measurements. This would offer a good opportunity to understand the underlying degradation mechanism. In addition, we appeal to give more descriptions of the fabrication process. For example, it needs to notify the lab conditions, such as chemistry laboratory or cleanroom. For the cleanroom, the classifications (by using International or US federal

Table 3 Comparisons of MPPT in high-performance IPSCs based on rigid substrates.

| Label	Illumination	Atmosphere	Temperature (°C)	Encapsulation	Performance	Ref.
a. Single-junction cells						
1	White LED (100 mW cm^{-2})	N_2	25	No	Retained 98% of initial PCE after 1500 h	27
2	White LED (100 mW cm^{-2})	Air 50 ± 10% RH	65	Yes	T_{80} = 1190 h	26
3	UV filter (420 nm) AM1.5 (100 mW cm^{-2})	N_2	~40	Yes	No degradation for 1000 h	3
4	White LED (100 mW cm^{-2})	N_2	45	Yes	Retained 93% of initial PCE after 1000 h, T_{80} = 3982 h	105
5	Plasma lamp AM1.5 (100 mW cm^{-2})	Air 40 ± 10% RH	~60	Yes	No efficiency loss after 550 h	25
6	AM1.5 (100 mW cm^{-2})	Air	~40	Yes	Retained 95% of initial PCE after 500 h	6
7	White LED (100 mW cm^{-2})	/	55 ± 5	No	Retained 90.5% of initial PCE after 1000 h	5
8	Plasma lamp AM1.5 (100 mW cm^{-2})	Air 60 ± 10% RH	~65	Yes	Retained 96.8% of initial PCE after 1200 h	17
/	UV filter (350 nm) Metal halide lamp AM1.5 (100 mW cm^{-2})	N_2	25	No	T_{80} = 3582 h	72
b. Monolithic tandem cells						
Perovskite/Si						
1	Dichromatic LED (100 mW cm^{-2})	Air 30–40% RH	25	No	Retained 95.5% of initial PCE after 300 h	9
2	Metal halide lamp AM 1.5 (100 mW cm^{-2})	Air 40–50% RH	40	Yes	Retained initial PCE after 400 h	30
Perovskite/CIGS						
3	Xenon lamp AM1.5 (100 mW cm^{-2})	Air	30	No	Retained over 88% of initial PCE after 500 h	36
Perovskite/perovskite						
4	Xenon lamp AM1.5 (100 mW cm^{-2})	Air 30–40% RH	54–60	No	Retained 88% of initial PCE after 500 h	43
5	Multicolor LED simulator AM 1.5 (100 mW cm^{-2})	Air 30–40% RH	30	Yes	Retained 90% of initial PCE after 600 h	44
c. Minimodules						
1	Xenon lamp AM1.5 (100 mW cm^{-2})	Air ~40 ± 10 % RH	~50	Yes	Retained 85% of initial PCE after 1000 h	25
2	Metal halide lamp AM1.5 (100 mW cm^{-2})	/	50 ± 5	Yes	Retained 93.6% of its initial PCE after 1056 h	50
3	White-light LED (100 mW cm^{-2})	Air	50–55	Yes	Retained 95% of the initial PCE after 1187 h	13
4	AM1.5 (100 mW cm^{-2})	Air 60% RH	50	Yes	Retained 90% of its initial PCE after 250 h	49
5	Metal halide lamp AM1.5 (100 mW cm^{-2})	/	/	Yes	Retained 87% of the initial PCE after 1000 h	47
6	UV filter (420 nm) Light test system (BIR-50, Bunkoh-Keiki Co., LTD) Xenon lamp AM 1.5 (100 mW cm^{-2})	Air	60	Yes	Retained 91% of its initial efficiency after 1000 h	46

LED denotes light-emitting diode. AM 1.5 indicates air mass 1.5. RH denotes relative humidity. T_{80} denotes the lifetime at 80% of the initial efficiency.

standards) should be given. Besides, the details of the used chemicals (e.g., the lot number) need to be considered since the material impurity is one of the unstable issues. We believe that these efforts will increase the reproducibility and development of the whole IPSC community.

b. In terms of the solution-processed devices, the atmosphere effect, no matter in a glove box, dry box, or even in a fume hood, is a crucial factor for the final performance stability. For mass production, the fabrication processes will inevitably involve a large volume of solvents. Even if introducing the so-called green or environmentally friendly solvents, these solvents will affect perovskite growth and film stability. Therefore, we must supervise the solvent influence in the actual workshop (e.g., increase the sensor to detect and track the real-time solvent concentration).

c. The stability measurement (e.g., the operational stability) needs to adopt standard facilities (e.g., consistently or uniformly approved light sources and generally accepted calibration method). To benefit inter-laboratory comparison, the details (e.g., the spectrum) of light sources should be given, in case of a mismatch from different suppliers. Due to the cost-effectiveness (low price with a several-year lifespan), the white LED is still a typical illumination source and its intensity calibration is also quite straightforward by comparing the device J_{SC} with a standard solar simulator.
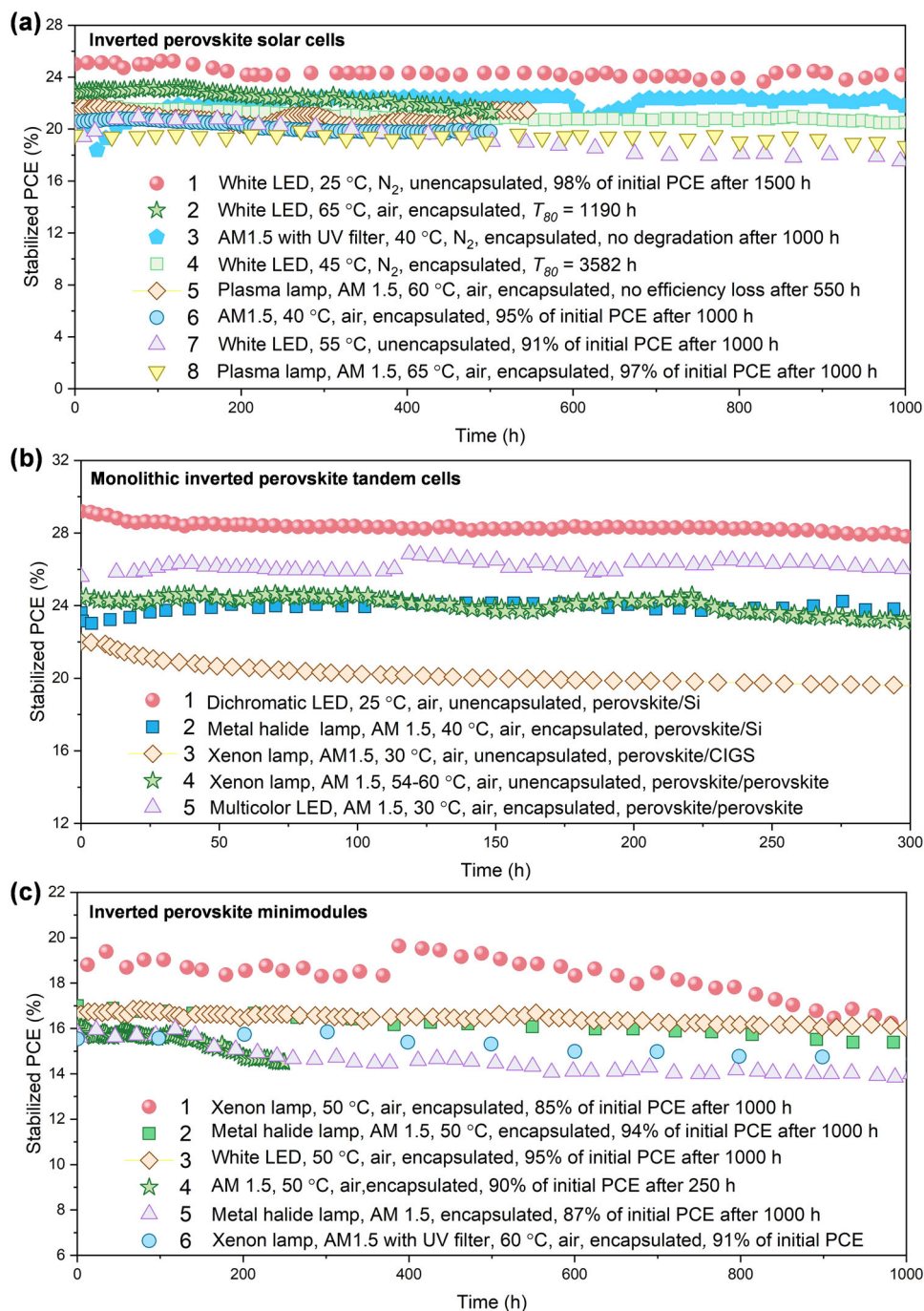
Fig. 4 The summary of operational stability of IPSCs based on MPPT results. a Small-area single-junction cells. **b** Tandem cells. **c** Minimodules. Note that all these devices are based on rigid substrates. The initial efficiency of sample 1 in (**a**) is unclear so we use the claimed champion PCE of 25% for reference. For each point, the data were extracted from the representative works (see details in Table 3). LED denotes light-emitting diode. AM 1.5 indicates air mass 1.5. T_{80} denotes the lifetime at 80% of the initial efficiency.

Apart from white-LED stability, the UV or Infrared (IR) stability can be separately studied by using the particular UV or IR illumination since AM 1.5 spectrum contains these parts. Thus, the detailed wavelength and intensity of UV or IR light are required. We thus appeal to display the operational stability, at least to show the performance stability under a white LED (minimum requirement). To approach industrial standards, the assessment of operational stability could combine the damp-heat test and MPPT in future studies.

Further research regarding the durability of devices for industrial commercialization would be worthwhile. With the collective efforts of academia and industry, there will be a bright prospect for IPSCs. For future applications, the inverted perovskite tandem modules are most promising. For example, the perovskite/Si modules could replace Si in solar farms and roof-integrated panels whilst the perovskite/CIGS modules can be used in spacecraft and interstellar probes. Associating with the advance of inverted perovskite modules, these products could compensate for power consumption in our daily life.

References

1. Gielen, D. et al. The role of renewable energy in the global energy transformation. *Energy Strateg. Rev.* **24**, 38–50 (2019).
2. Luo, D. et al. Enhanced photovoltage for inverted planar heterojunction perovskite solar cells. *Science* **360**, 1442–1446 (2018). **(This study verified the high open-circuit voltage of over 1.2 V in the inverted perovskite solar cells)**.
3. Zheng, X. et al. Managing grains and interfaces via ligand anchoring enables 22.3%-efficiency inverted perovskite solar cells. *Nat. Energy* **5**, 131–140 (2020).
4. Li, F. et al. Regulating surface termination for efficient inverted perovskite solar cells with greater than 23% efficiency. *J. Am. Chem. Soc.* **142**, 20134–20142 (2020).
5. Xiaodong, L. et al. Constructing heterojunctions by surface sulfidation for efficient inverted perovskite solar cells. *Science* **375**, 434–437 (2022).
6. Randi, A. et al. Damp heat-stable perovskite solar cells with tailored-dimensionality 2D/3D heterojunctions. *Science* **376**, 73–77 (2022).
7. Bush, K. A. et al. 23.6%-efficient monolithic perovskite/silicon tandem solar cells with improved stability. *Nat. Energy* **2**, 17009 (2017).
8. Richter, A. et al. Reassessment of the limiting efficiency for crystalline silicon solar cells. *IEEE J. Photovoltaics* **3**, 1184–1191 (2013).
9. Al-Ashouri, A. et al. Monolithic perovskite/silicon tandem solar cell with >29% efficiency by enhanced hole extraction. *Science* **370**, 1300–1309 (2020).
10. Li, H. et al. Perovskite tandem solar cells: from fundamentals to commercial deployment. *Chem. Rev.* **120**, 9835–9950 (2020).
11. Miyazawa, Y. et al. Tolerance of perovskite solar cell to high-energy particle irradiations in space environment. *iScience* **2**, 148–155 (2018).
12. Hoang, M. T. et al. Are metal halide perovskite solar cells ready for space applications? *J. Phys. Chem. Lett.* **13**, 2908–2920 (2022).
13. Zhichun, Y. et al. Slot-die coating large-area formamidinium-cesium perovskite film for efficient and stable parallel solar module. *Sci. Adv.* **7**, eabg3749 (2021).
14. Kaltenbrunner, M. et al. Flexible high power-per-weight perovskite solar cells with chromium oxide-metal contacts for improved stability in air. *Nat. Mater.* **14**, 1032–1039 (2015).
15. Yoon, J. et al. Superflexible, high-efficiency perovskite solar cells utilizing graphene electrodes: towards future foldable power sources. *Energy Environ. Sci.* **10**, 337–345 (2017).
16. Lin, Y. H. et al. A piperidinium salt stabilizes efficient metal-halide perovskite solar cells. *Science.* **369**, 96–102 (2020). **(This study achieved highly stable inverted perovskite solar cells)**.
17. Yang, S. et al. Stabilizing halide perovskite surfaces for solar cell operation with wide-bandgap lead oxysalts. *Science* **365**, 473–478 (2019).
18. Wang, J. et al. Highly efficient all-inorganic perovskite solar cells with suppressed non-radiative recombination by a Lewis base. *Nat. Commun.* **11**, 177 (2020).
19. Liang, C. et al. Two-dimensional Ruddlesden-Popper layered perovskite solar cells based on phase-pure thin films. *Nat. Energy* **6**, 38–45 (2021).
20. Rao, L. et al. Wearable Tin-based perovskite solar cells achieved by a crystallographic size effect. *Angew. Chemie Int. Ed.* **60**, 14693–14700 (2021).
21. Jiang, X. et al. Tin halide perovskite solar cells: an emerging thin-film photovoltaic technology. *Accounts Mater. Res.* **2**, 210–219 (2021).
22. Jeng, J. Y. et al. $CH_3NH_3PbI_3$ perovskite/fullerene planar-heterojunction hybrid solar cells. *Adv. Mater.* **25**, 3727–3732 (2013). **(The first study created the inverted perovskite solar cells)**.
23. Nie, W. et al. High-efficiency solution-processed perovskite solar cells with millimeter-scale grains. *Science.* **347**, 522–525 (2015).
24. Zheng, X. et al. Defect passivation in hybrid perovskite solar cells using quaternary ammonium halide anions and cations. *Nat. Energy* **2**, 17102 (2017).
25. Shangshang, C. et al. Stabilizing perovskite-substrate interfaces for high-performance perovskite modules. *Science.* **373**, 902–907 (2021).
26. Chen, H. et al. Quantum-size-tuned heterostructures enable efficient and stable inverted perovskite solar cells. *Nat. Photon.* **16**, 352–358 (2022).
27. Zhen, L. et al. Organometallic-functionalized interfaces for highly efficient inverted perovskite solar cells. *Science* **376**, 416–420 (2022). **(This study achieved the champion performance in the inverted perovskite solar cells)**.
28. Mazzarella, L. et al. Infrared light management using a nanocrystalline silicon oxide interlayer in monolithic perovskite/silicon heterojunction tandem solar cells with efficiency above 25%. *Adv. Energy Mater.* **9**, 1803241 (2019).
29. Köhnen, E. et al. Highly efficient monolithic perovskite silicon tandem solar cells: analyzing the influence of current mismatch on device performance. *Sustain. Energy Fuels* **3**, 1995–2005 (2019).
30. Hou, Y. et al. Efficient tandem solar cells with solution-processed perovskite on textured crystalline silicon. *Science* **367**, 1135–1140 (2020).
31. Xu, J. et al. Triple-halide wide-band gap perovskites with suppressed phase segregation for efficient tandems. *Science* **367**, 1097–1104 (2020).
32. Kim, D. et al. Efficient, stable silicon tandem cells enabled by anion-engineered wide-bandgap perovskites. *Science* **368**, 155–160 (2020).
33. Oxford PV retakes tandem solar cell efficiency record—pv magazine International. https://www.pv-magazine.com/2020/12/21/oxford-pv-retakes-tandem-cell-efficiency-record/ (2022).
34. Helmholtz Center achieves 29.80% efficiency for perovskite/silicon tandem solar cell—pv magazine International. https://www.pv-magazine.com/2021/11/22/helmholtz-center-achieves-29-80-efficiency-for-perovskite-silicon-tandem-solar-cell/ (2022).
35. Jiang, L. et al. Efficient and stable perovskite-silicon tandem solar cells through contact displacement by MgF_x. *Science* **367**, 302–306 (2020).
36. Qifeng, H. et al. High-performance perovskite/$Cu(In,Ga)Se_2$ monolithic tandem solar cells. *Science* **361**, 904–908 (2018).
37. Jošt, M. et al. 21.6%-Efficient monolithic perovskite/$Cu(In,Ga)Se_2$ tandem solar cells with thin conformal hole transport layers for integration on rough bottom cell surfaces. *ACS Energy Lett.* **4**, 583–590 (2019).
38. Al-Ashouri, A. et al. Conformal monolayer contacts with lossless interfaces for perovskite single junction and monolithic tandem solar cells. *Energy Environ. Sci.* **12**, 3356–3369 (2019).
39. Jošt, M. et al. Perovskite/CIGS tandem solar cells: from certified 24.2% toward 30% and beyond. *ACS Energy Lett.* **7**, 1298–1307 (2022).
40. Eperon, G. E. et al. Perovskite-perovskite tandem photovoltaics with optimized band gaps. *Science* **354**, 861–865 (2016).
41. Zhao, D. et al. Efficient two-terminal all-perovskite tandem solar cells enabled by high-quality low-bandgap absorber layers. *Nat. Energy* **3**, 1093–1100 (2018).
42. Palmstrom, A. F. et al. Enabling flexible all-perovskite tandem solar cells. *Joule* **3**, 2193–2204 (2019).
43. Xiao, K. et al. All-perovskite tandem solar cells with 24.2% certified efficiency and area over 1 cm^2 using surface-anchoring zwitterionic antioxidant. *Nat. Energy* **5**, 870–880 (2020).
44. Lin, R. et al. All-perovskite tandem solar cells with improved grain surface passivation. *Nature* **603**, 73–78 (2022).
45. Deng, Y. et al. Surfactant-controlled ink drying enables high-speed deposition of perovskite films for efficient photovoltaic modules. *Nat. Energy* **3**, 560–566 (2018).
46. Bi, E. et al. Efficient perovskite solar cell modules with high stability enabled by iodide diffusion barriers. *Joule* **3**, 2748–2760 (2019).
47. Yehao, D. et al. Tailoring solvent coordination for high-speed, room-temperature blading of perovskite photovoltaic films. *Sci. Adv.* **5**, eaax7537 (2019).
48. Deng, Y. et al. Reduced self-doping of perovskites induced by short annealing for efficient solar modules. *Joule* **4**, 1949–1960 (2020).
49. Huang, H. H. et al. A simple one-step method with wide processing window for high-quality perovskite mini-module fabrication. *Joule* **5**, 958–974 (2021).
50. Deng, Y. et al. Defect compensation in formamidinium-caesium perovskites for highly efficient solar mini-modules with improved photostability. *Nat. Energy* **6**, 633–641 (2021).
51. Zhang, M. et al. Electrode design to overcome substrate transparency limitations for highly efficient 1 cm^2 mesoscopic perovskite solar cells. *Joule* **2**, 2694–2705 (2018).
52. Cheacharoen, R. et al. Design and understanding of encapsulated perovskite solar cells to withstand temperature cycling. *Energy Environ. Sci.* **11**, 144–150 (2017).
53. Zhang, J. et al. High-performance ITO-free perovskite solar cells enabled by single-walled carbon nanotube films. *Adv. Funct. Mater.* **31**, 2104396 (2021).
54. Back, H. et al. Achieving long-term stable perovskite solar cells via ion neutralization. *Energy Environ. Sci.* **9**, 1258–1263 (2016).
55. Deng, Y. et al. Air-stable, efficient mixed-cation perovskite solar cells with Cu electrode by scalable fabrication of active layer. *Adv. Energy Mater.* **6**, 1600372 (2016).
56. Zhao, J. et al. Is Cu a stable electrode material in hybrid perovskite solar cells for a 30-year lifetime? *Energy Environ. Sci.* **9**, 3650–3656 (2016).
57. Guerrero, A. et al. Interfacial degradation of planar lead halide perovskite solar cells. *ACS Nano* **10**, 218–224 (2016).
58. Boyd, C. C. et al. Barrier design to prevent metal-induced degradation and improve thermal stability in perovskite solar cells. *ACS Energy Lett* **3**, 1772–1778 (2018).
59. Bai, S. et al. Planar perovskite solar cells with long-term stability using ionic liquid additives. *Nature* **571**, 245–250 (2019).
60. Babu, V. et al. Improved stability of inverted and flexible perovskite solar cells with carbon electrode. *ACS Appl. Energy Mater.* **3**, 5126–5134 (2020).

61. Seo, S. et al. Perovskite solar cells with inorganic electron- and hole-transport layers exhibiting long-term (≈500 h) stability at 85 °C under continuous 1 sun illumination in ambient Air. *Adv. Mater.* **30**, 1801010 (2018).

62. Wu, W. Q. et al. Molecular doping enabled scalable blading of efficient hole-transport-layer-free perovskite solar cells. *Nat. Commun.* **9**, 1625 (2018).

63. Wang, Q. et al. Doped hole transport layer for efficiency enhancement in planar heterojunction organolead trihalide perovskite solar cells. *Nano Energy* **15**, 275–280 (2015).

64. Boyd, C. C. et al. Understanding degradation mechanisms and improving stability of perovskite photovoltaics. *Chem. Rev* **119**, 3418–3451 (2018). (**A detailed paper for the introduction of the stability**).

65. Thampy, S. et al. Metal oxide-induced instability and its mitigation in halide perovskite solar cells. *J. Phys. Chem. Lett.* **12**, 8495–8506 (2021).

66. Di Girolamo, D. et al. Stability and dark hysteresis correlate in NiO-based perovskite solar cells. *Adv. Energy Mater.* **9**, 1901642 (2019).

67. Chen, H. et al. Efficient and stable inverted perovskite solar cells incorporating secondary amines. *Adv. Mater.* **31**, 1903559 (2019).

68. Boyd, C. C. et al. Overcoming redox reactions at perovskite-nickel oxide interfaces to boost voltages in perovskite solar cells. *Joule* **4**, 1759–1775 (2020).

69. Kim, J. H. et al. High-performance and environmentally stable planar heterojunction perovskite solar cells based on a solution-processed copper-doped nickel oxide hole-transporting layer. *Adv. Mater.* **27**, 695–701 (2015).

70. Zhao, D. et al. High-efficiency solution-processed planar perovskite solar cells with a polymer hole transport layer. *Adv. Energy Mater.* **5**, 1401855 (2014).

71. Chang, C. Y. et al. Facile fabrication of self-assembly functionalized polythiophene hole transporting layer for high performance perovskite solar cells. *Adv. Sci.* **8**, 2002718 (2021).

72. Aktas, E. et al. Understanding the perovskite/self-assembled selective contact interface for ultra-stable and highly efficient p-i-n perovskite solar cells. *Energy Environ. Sci.* **14**, 3976–3985 (2021).

73. Wang, Z. et al. Stability of perovskite solar cells: a prospective on the substitution of the Acation and X anion. *Angew. Chemie Int. Ed.* **56**, 1190–1212 (2017).

74. Aristidou, N. et al. Fast oxygen diffusion and iodide defects mediate oxygen-induced degradation of perovskite solar cells. *Nat. Commun.* **8**, 1–10 (2017).

75. Chen, B. et al. Imperfections and their passivation in halide perovskite solar cells. *Chem. Soc. Rev.* **48**, 3842–3867 (2019). (**This paper systematically discussed a plethora of defects and passivation methods in perovskite solar cells**).

76. Shao, Y. et al. Origin and elimination of photocurrent hysteresis by fullerene passivation in CH$_3$NH$_3$PbI$_3$ planar heterojunction solar cells. *Nat. Commun.* **5**, 1–7 (2014). (**This study explained why the inverted perovskite solar cells have negligible hysteresis and disclosed the passivation function of the fullerene electron transport layer**).

77. Chambon, S. et al. Photo- and thermal degradation of MDMO-PPV:PCBM blends. *Sol. Energy Mater. Sol. Cells* **91**, 394–398 (2007).

78. Shibayama, N. et al. Design of BCP buffer layer for inverted perovskite solar cells using ideal factor. *APL Mater.* **7**, 31117 (2019).

79. Gommans, H. et al. On the role of bathocuproine in organic photovoltaic cells. *Adv. Funct. Mater.* **18**, 3686–3691 (2008).

80. Chen, W. et al. Metal acetylacetonate series in interface engineering for full low-temperature-processed, high-performance, and stable planar perovskite solar cells with conversion efficiency over 16% on 1 cm^2 scale. *Adv. Mater.* **29**, 1603923 (2017).

81. Wu, S. et al. 2D metal–organic framework for stable perovskite solar cells with minimized lead leakage. *Nat. Nanotechnol.* **15**, 934–940 (2020).

82. Wang, J. et al. Tuning an electrode work function using organometallic complexes in inverted perovskite solar cells. *J. Am. Chem. Soc.* **143**, 7759–7768 (2021).

83. Bai, Y. et al. Interface engineering for highly efficient and stable planar p-i-n perovskite solar cells. *Adv. Energy Mater.* **8**, 1701883 (2017).

84. Li, B. et al. Tailoring perovskite adjacent interfaces by conjugated polyelectrolyte for stable and efficient solar cells. *Sol. RRL* **4**, 2000060 (2020).

85. Zhenyi, N. et al. Resolving spatial and energetic distributions of trap states in metal halide perovskite solar cells. *Science* **367**, 1352–1358 (2020).

86. Yang, X. et al. Buried interfaces in halide perovskite photovoltaics. *Adv. Mater.* **33**, 2006435 (2021). (**This study visualized the buried interface under the perovskite**).

87. Stolterfoht, M. et al. Visualization and suppression of interfacial recombination for high-efficiency large-area pin perovskite solar cells. *Nat. Energy* **3**, 847–854 (2018). (**This study disclosed the significance of interfacial recombination in inverted perovskite solar cells**).

88. Kim, J. H. et al. Understanding mechanical behavior and reliability of organic electronic materials. *MRS Bull* **42**, 115–123 (2017).

89. Zhenghong, D. et al. Interfacial toughening with self-assembled monolayers enhances perovskite solar cell reliability. *Science* **372**, 618–622 (2021).

90. Bai, Y. et al. Enhancing stability and efficiency of perovskite solar cells with crosslinkable silane-functionalized and doped fullerene. *Nat. Commun.* **7**, 12806 (2016).

91. Zhang, M. et al. Reconfiguration of interfacial energy band structure for high-performance inverted structure perovskite solar cells. *Nat. Commun.* **10**, 4593 (2019).

92. Jung, S. K. et al. Nonfullerene electron transporting material based on naphthalene diimide small molecule for highly stable perovskite solar cells with efficiency exceeding 20%. *Adv. Funct. Mater.* **28**, 1800346 (2018).

93. Chen, W. et al. N-type conjugated polymer as efficient electron transport layer for planar inverted perovskite solar cells with power conversion efficiency of 20.86%. *Nano Energy* **68**, 104363 (2020).

94. Jin Wook, L. et al. Rethinking the A cation in halide perovskites. *Science* **375**, eabj1186 (2022).

95. Chen, Q. et al. Rapid microwave-annealing process of hybrid perovskites to eliminate miscellaneous phase for high performance photovoltaics. *Adv. Sci.* **7**, 2000480 (2020).

96. Chen, S. et al. Identifying the soft nature of defective perovskite surface layer and its removal using a facile mechanical approach. *Joule* **4**, 2661–2674 (2020).

97. Wang, Q. et al. Thin insulating tunneling contacts for efficient and water-resistant perovskite solar cells. *Adv. Mater.* **28**, 6734–6739 (2016).

98. Wu, S. et al. A chemically inert bismuth interlayer enhances long-term stability of inverted perovskite solar cells. *Nat. Commun.* **10**, 1161 (2019).

99. Xiaodong, L. et al. Chemical anti-corrosion strategy for stable inverted perovskite solar cells. *Sci. Adv.* **6**, eabd1580 (2022).

100. Liu, Y. et al. Ultrahydrophobic 3D/2D fluoroarene bilayer-based water-resistant perovskite solar cells with efficiencies exceeding 22%. *Sci. Adv.* **5**, eaaw2543 (2019).

101. Lin, C. T. et al. Enhancing the operational stability of unencapsulated perovskite solar cells through Cu-Ag bilyer electrode incorporation. *J. Mater. Chem. A* **8**, 8684–8691 (2020).

102. Chen, B. et al. Passivation of the buried interface via preferential crystallization of 2D perovskite on metal oxide transport layers. *Adv. Mater.* **33**, 2103394 (2021).

103. Xiong, S. et al. Direct observation on p- to n-type transformation of perovskite surface region during defect passivation driving high photovoltaic efficiency. *Joule* **5**, 467–480 (2021).

104. Solanki, A. et al. Heavy water additive in formamidinium: a novel approach to enhance perovskite solar cell efficiency. *Adv. Mater.* **32**, 1907864 (2020).

105. Cao, Q. et al. Star-polymer multidentate-cross-linking strategy for superior operational stability of inverted perovskite solar cells at high efficiency. *Energy Environ. Sci.* **14**, 5406–5415 (2021).

106. Wu, W. Q. et al. Bilateral alkylamine for suppressing charge recombination and improving stability in blade-coated perovskite solar cells. *Sci. Adv.* **5**, eaav8925 (2019).

107. Chen, K. et al. Defect passivation by alcohol-soluble small molecules for efficient p-i-n planar perovskite solar cells with high open-circuit voltage. *J. Mater. Chem. A* **7**, 21140–21148 (2019).

108. Chen, H. et al. Organic n-type molecule: managing the electronic states of bulk perovskite for high-performance photovoltaics. *Adv. Funct. Mater.* **30**, 2001788 (2020).

109. Wang, X. et al. Engineering fluorinated-cation containing inverted perovskite solar cells with an efficiency of >21% and improved stability towards humidity. *Nat. Commun.* **12**, 52 (2021).

110. Shangshang, C. et al. Iodine reduction for reproducible and high-performance perovskite solar cells and modules. *Sci. Adv.* **7**, eabe8130 (2022).

111. Yang, D. et al. Achieving 20% efficiency for low-temperature-processed inverted perovskite solar cells. *Adv. Funct. Mater.* **29**, 1807556 (2019).

112. Sun, X. et al. Efficient inverted perovskite solar cells with low voltage loss achieved by a pyridine-based dopant-free polymer semiconductor. *Angew. Chemie Int. Ed.* **60**, 7227–7233 (2021).

113. Cai, N. et al. Synergistical dipole-dipole interaction induced self-assembly of phenoxazine-based hole-transporting materials for efficient and stable inverted perovskite solar cells. *Angew. Chemie Int. Ed.* **60**, 20437–20442 (2021).

114. Wang, S. et al. Critical role of removing impurities in nickel oxide on high-efficiency and long-term stability of inverted perovskite solar cells. *Angew. Chemie Int. Ed.* **61**, e202116534 (2022).

115. Matteo, D. et al. 23.7% Efficient inverted perovskite solar cells by dual interfacial modification. *Sci. Adv.* **7**, eabj7930 (2022).

116. Hu, Q. et al. Improving efficiency and stability of perovskite solar cells enabled by a near-infrared-absorbing moisture barrier. *Joule* **4**, 1575–1593 (2020).

117. Wu, S. et al. Modulation of defects and interfaces through alkylammonium interlayer for efficient inverted perovskite solar cells. *Joule* **4**, 1248–1262 (2020).

118. Zhou, Q. et al. Multifunctional chemical bridge and defect passivation for highly efficient inverted perovskite solar cells. *ACS Energy Lett.* **6**, 1596–1606 (2021).

119. Liu, X. et al. Shallow defects levels and extract detrapped charges to stabilize highly efficient and hysteresis-free perovskite photovoltaic devices. *Nano Energy* **71**, 104556 (2020).

120. Khenkin, M. V. et al. Consensus statement for stability assessment and reporting for perovskite photovoltaics based on ISOS procedures. *Nat. Energy* **5**, 35–49 (2020). **(This paper summarized a series of protocols for stability testing of perovskite solar cells).**

121. Li, N. et al. Towards commercialization: the operational stability of perovskite solar cells. *Chem. Soc. Rev.* **49**, 8235–8286 (2020).

122. Habisreutinger, S. N. et al. Hysteresis index: a figure without merit for quantifying hysteresis in perovskite solar cells. *ACS Energy Lett.* **3**, 2472–2476 (2018).

123. Holzhey, P. et al. A full overview of international standards assessing the long-term stability of perovskite solar cells. *J. Mater. Chem. A* **6**, 21794–21808 (2018).

124. Lang, F. et al. Proton radiation hardness of perovskite tandem photovoltaics. *Joule* **4**, 1054–1069 (2020).

125. Ma, S. et al. Development of encapsulation strategies towards the commercialization of perovskite solar cells. *Energy Environ. Sci.* **15**, 13–55 (2022).

Author contributions

B.L. and W.Z. conceived of the work. B.L. wrote the first draft and W.Z. revised the paper. W.Z. directed and supervised the project.

Competing interests

The authors declare no competing interests.

Additional information

Supplementary information The online version contains supplementary material available at https://doi.org/10.1038/s43246-022-00291-x.

Correspondence and requests for materials should be addressed to Wei Zhang.

Peer review information *Communications Materials* thanks the anonymous reviewers for their contribution to the peer review of this work. Primary Handling Editors: Marta Haro and John Plummer. Peer reviewer reports are available.

Reprints and permission information is available at http://www.nature.com/reprints

Publisher's note Springer Nature remains neutral with regard to jurisdictional claims in published maps and institutional affiliations.